5620 J. Med. Chem. 2010, 53, 5620–5628
DOI: 10.1021/jm100634a

Journal of Medicinal Chemistry Article

Discovery of 6-(Aminomethyl)-5-(2,4-dichlorophenyl)-7-methylimidazo[1,2-*a*]pyrimidine-2-carboxamides as Potent, Selective Dipeptidyl Peptidase-4 (DPP4) Inhibitors

Wei Meng,*,† Robert P. Brigance,† Hannguang J. Chao,† Aberra Fura,§ Thomas Harrity,‡ Jovita Marcinkeviciene,∥ Stephen P. O'Connor,† James K. Tamura,⊥ Dianlin Xie,⊥ Yaqun Zhang,⊥ Herbert E. Klei,⊥ Kevin Kish,⊥ Carolyn A. Weigelt,# Huji Turdi,† Aiying Wang,‡ Robert Zahler,† Mark S. Kirby,‡ and Lawrence G. Hamann†

†*Departments of Discovery Chemistry,* ‡*Metabolic Diseases,* §*Pharmaceutical Candidate Optimization,* ∥*Chemical Enzymology,* ⊥*Gene Expression & Protein Biochemistry, and* #*Computer-Assisted Drug Design, Bristol-Myers Squibb, Research and Development, P.O. Box 5400, Princeton, New Jersey 08543-5400*

Received May 25, 2010

Continued structure−activity relationship (SAR) exploration within our previously disclosed azolopyrimidine containing dipeptidyl peptidase-4 (DPP4) inhibitors led us to focus on an imidazolopyrimidine series in particular. Further study revealed that by replacing the aryl substitution on the imidazole ring with a more polar carboxylic ester or amide, these compounds displayed not only increased DPP4 binding activity but also significantly reduced human ether-à-go-go related gene (hERG) and sodium channel inhibitory activities. Additional incremental adjustment of polarity led to permeable molecules which exhibited favorable pharmacokinetic (PK) profiles in preclinical animal species. The active site binding mode of these compounds was determined by X-ray crystallography as exemplified by amide **24c**. A subsequent lead molecule from this series, (+)-6-(aminomethyl)-5-(2,4-dichlorophenyl)-*N*-(1-ethyl-1*H*-pyrazol-5-yl)-7-methylimidazo[1,2-*a*]pyrimidine-2-carboxamide (**24s**), emerged as a potent, selective DPP4 inhibitor that displayed excellent PK profiles and in vivo efficacy in *ob*/*ob* mice.

Introduction

Glucogon-like peptide-1 (GLP-1[a]) based therapeutics have emerged in the recent years as novel and promising treatments for type 2 diabetes.[1] Upon ingestion of meals, the incretin hormone GLP-1 (7−36), the active and natural form of GLP-1, is secreted from intestinal L-cells where it then stimulates insulin secretion, inhibits glucogon release, delays gastric emptying, and promotes β-cell trophism, all benefiting glucose homeostasis in both animal models and human.[2] GLP-1 levels in type 2 diabetics are markedly reduced, but exogenous GLP-1 infusion can lead to normal insulin response to glucose,[3] thereby forming the basis for GLP-1 and its analogues as novel treatments of type 2 diabetes. Exenatide, a GLP-1 analogue, was approved by the FDA in 2005 for treating type 2 diabetes.[4]

GLP-1 (7−36) is the most potent incretin hormone with a half-maximal effective concentration of 10 pM for its effects on pancreatic β-cells.[5] For GLP-1 (7−36) to exert its biological functions, it must circulate and bind to the GLP-1 receptor, which is highly expressed in pancreatic β-cells. Following secretion under normal physiological conditions, GLP-1 (7−36) is rapidly degraded by DPP4 (EC 3.4.14.5) to afford inactive GLP-1 (9−36). This quick inactivation process leads to an apparent half-life of 60−90 s for GLP-1 (7−36), and there is evidence that less than 50% of released active GLP-1 (7−36) can reach circulation because of this natural degradation mechanism.[6] It is therefore apparent that a DPP4 inhibitor can prevent degradation of and lead to potentiation of GLP-1, which will further improve glucose and insulin homeostasis.[7] DPP4 is a nonclassical, sequence-specific serine protease that is ubiquitously expressed throughout the body. Membrane-bound DPP4 is especially highly expressed in the endothelium of the capillary bed in close proximity to intestinal L-cells where GLP-1 is secreted. There is also a soluble form of DPP4 circulating in plasma, although this form plays little role in the cleavage of GLP-1.[8] A number of small molecule DPP4 inhibitors, including vildagliptin **1** (approved in Europe, Brazil, and Mexico),[9] sitagliptin **2**,[10] and saxagliptin **3**,[11] have been granted regulatory approval, and alogliptin **4** (Figure 1) has been advanced to late stage human clinical trials.[12] Each of these agents has demonstrated an ability to lower blood glucose and HbA1c levels and to improve glucose tolerance in type 2 diabetic patients.[13]

By building on a successful DPP4 program that discovered saxagliptin, at BMS, we continued to expand our medicinal chemistry efforts at discovering novel scaffolds that can act as DPP4 inhibitors. From a previous report from our laboratories,[14] we discovered several novel series of azolopyrimidine amines as DPP4 inhibitors which were intrinsically potent at DPP4 and selective over the other dipeptidyl peptidase (DPP) family of enzymes (see compound **5**, Figure 1 as an example). Most of the structures in these series contain an aromatic or heteroaromatic group on the azolo ring, and this substitution

*To whom correspondence should be addressed. Phone: 609-818-4976. Fax: 609-818-3550. E-mail: wei.meng@bms.com.

[a] Abbreviations: DPP4, dipeptidyl peptidase-4; GLP-1, glucogon-like peptide-1; DPP, dipeptidyl peptidase; hERG, human ether-à-go-go related gene; SAR, structure−activity relationship; PK, pharmacokinetic; $KMnO_4$, potassium permanganate; TFA, trifluoroacetic acid; MsCl, methanesulfonyl chloride; NaN_3, sodium azide; PPh_3, triphenyl phosphine; EDAC, 1-ethyl-3-(3-dimethylaminopropyl)carbodiimide hydrochloride; HOAt, 1-hydroxy-7-azabenzotriazole; PD, pharmacodynamic; PAMPA, parallel membrane permeability assays; oGTT, oral glucose tolerance test; FAP, fibroblast activation protein; IA, intraarterial.

 Published on Web 07/15/2010

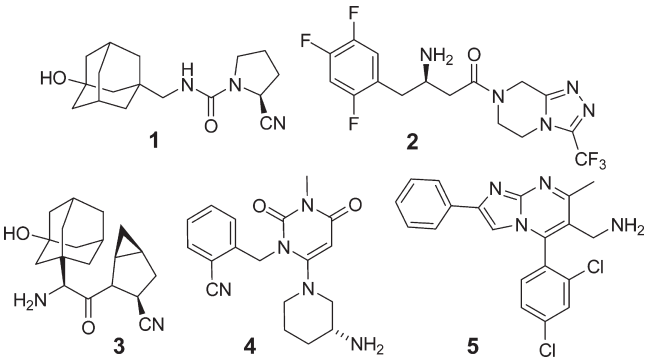

Figure 1. Structures of selected DPP4 inhibitors.

appeared to enhance the binding affinity to DPP4. However, all of these compounds also displayed high levels of the human ether-à-go-go related gene (hERG) and sodium channel inhibition. To minimize undesired channel activities by reducing lipophilicity, we sought to replace the aromatic or heteroaromatic group on the azolo ring with more polar functional groups. This structure−activity relationship (SAR) investigation led us to discover a series of imidazolopyrimidine amides as a highly potent and selective class of DPP4 inhibitors as represented by **24s**. Free of hERG and sodium channel activities, **24s** displayed an excellent balance of DPP4 binding activity, selectivity over other DPPs, in vivo efficacy, and pharmacokinetic (PK) profiles in several preclinical species that represents an advanced lead with drug-like properties as a potential treatment for type 2 diabetes.

Chemistry

Imidazolopyrimidine ester **19** was synthesized as shown in Scheme 1. Knoevenagel condensation of *t*-butylacetoacetate **6** and 2,4-dichlorobenzaldehyde **7** in 2-propanol with a catalytic amount of dimethylamine and acetic acid provided a 1:1 *E*/*Z* mixture of acrylate **8** in 67% yield. Condensation of 2-aminopyrimidine **9** with ethyl bromopyruvate **10** in ethanol at 75 °C gave imidazolopyrimidine **11** as a mixture of two regioisomers, which underwent hydrazine hydrate-mediated cleavage to afford substituted imidazole **12** in good overall yield.[15] Condensation of acrylate **8** and imidazole **12** in ethanol at 70 °C afforded substituted imidazolodihydropyrimidine **13**, which was immediately subjected to oxidation with $KMnO_4$ to give diester **14**. The *t*-butyl ester was next converted to an aminomethyl moiety in a five-step sequence. First, hydrolysis of the *t*-butylester of **14** with TFA afforded acid **15** quantitatively. Mixed anhydride formation of acid **15** with ethyl chloroformate, followed by reduction with $NaBH_4$, provided alcohol **16** in 45% yield. The alcohol was then treated with MsCl to form benzyl chloride **17**, which was converted to azide **18** using NaN_3. Final reduction of azide **18** with PPh_3 afforded the amine ester **19** in 50% yields for the three steps.

During our characterization of benzylamine **19**, as well as intermediates **16**, **17**, and **18**, it was noticed that the two benzylic protons next to the amino group existed as a pair of doublet of doublets in the proton NMR spectrum, indicating that these two protons are nonequivalent. This further suggested the possibility of restricted rotation along the biaryl bond and the existence of atropisomers. Variable temperature NMR up to 120 °C did not lead to coalescence of these doublets. When ester **19** was subjected to chiral HPLC methods, it became clear that two distinct compounds existed. Additional chemical and

Scheme 1[a]

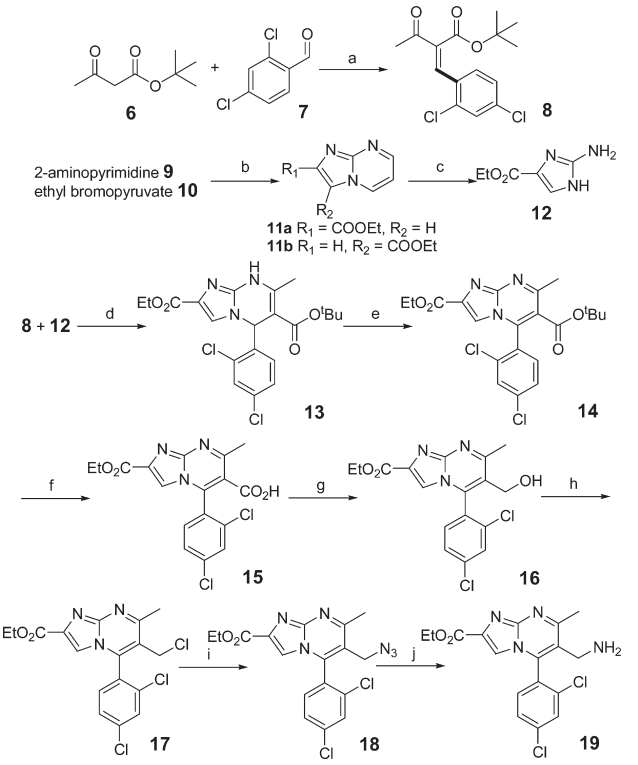

[a] Reagents: (a) AcOH, Me_2NH, IPA, 67%; (b) EtOH, 75 °C, 30% **11a**, 20% **11b**; (c) $NH_2NH_2 \cdot H_2O$, EtOH, 75 °C, 100%; (d) EtOH, 70 °C, 59%; (e) $KMnO_4$, acetone, 57%; (f) TFA, CH_2Cl_2, 100%; (g) ClCOOEt, Et_3N, THF, then $NaBH_4$, THF, H_2O, 0 °C, 45%; (h) MsCl, Et_3N, CH_2Cl_2; (i) NaN_3, DMF, 50 °C; (j) PPh_3, THF, H_2O, 50 °C, 50% for 3 steps.

instrumental analyses led to the conclusion that **19** is comprised of a pair of stable, noninterconverting enantiomers in which the chirality arises from atropisomerism. To more accurately assess their enzymatic activity, **19** was separated on a chiral HPLC column to give each atropisomer **20** and **21** (Figure 2). The absolute stereochemistry was assigned based on the X-ray crystal structure determination for an earlier intermediate **15** and later confirmed by X-ray crystallography in the active site of DPP4.

To improve upon the potentially poor metabolic stability of ethyl ester **19**, we set out to replace the ester moiety with metabolically more stable amides. To expedite SAR studies in this series, a combinatorial approach was taken to prepare these amides using a wide variety of sterically and electronically differentiated amines. In anticipation of different activity for the two enantiomers, most of the amides were synthesized as single atropisomers and only atropisomerically pure molecules were carried onto PK and pharmacodynamic (PD) studies. Because racemic azide **18** displayed superior separation behavior over **19** on chiral HPLC, a large amount of this intermediate **18** was processed to provide chrial azide **22**. Mild chemical conditions were employed for the subsequent steps to minimize any possible racemization. Therefore, the ethyl ester of **22** was saponified by LiOH to form acid **23**, which was then coupled with different amines using standard EDAC/HOAt conditions to afford the desired amides. A PPh_3-mediated reduction of the azide, followed by purification by preparatory HPLC, provided final products **24a**−**ee** (Scheme 2) as TFA salts in moderate to high yields. As analyzed by chiral HPLC, no interconversion of the atropisomers occurred during

the above chemical sequence. In addition, no racemization was observed when amides such as **24c** and **24s** were heated in water at 100 °C for up to 10 days.

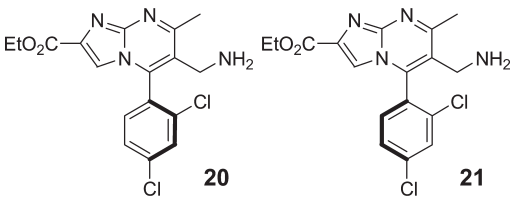

Figure 2. Structures of atropisomers **20** and **21**.

Scheme 2[a]

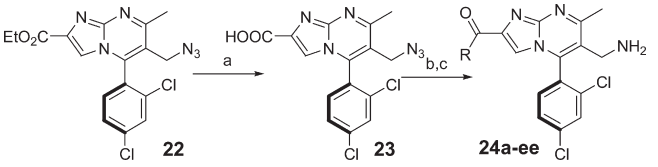

[a] Reagents: (a) $LiOH \cdot H_2O$, THF, H_2O, 94%; (b) EDAC, HOAt, amine, THF, $^iPr_2NEt$; (c) PPh_3, THF, H_2O, 50−90%.

Results and Discussion

The DPP4 inhibitory activity for compounds **19**−**21** and **24a**−**ee** is summarized in Table 1. Compounds were incubated with human recombinant DPP4 under steady state conditions to detect the cleavage of the pseudosubstrate, Gly-Pro-*p*NA. We were encouraged by the observation of subnanomolar DPP4 activity (K_i = 0.7 nM) for the first analogue that was prepared in this series, prototype ester **19**. Furthermore, upon separation of the two atropisomers, we observed that eutomer **21** was about 2-fold more potent than **19** with DPP4 K_i of 0.4 nM, whereas **20** was more than 10-fold less active, indicating most of the activity for **19** resided in one of its enantiomers. On the basis of this finding, all subsequent amides were prepared in the more active atropisomer series. All of the amide analogues exhibited excellent DPP4 inhibitory activity, with K_i's ranging from sub- to single-digit nanomolar. Steric and electronic effects did not appear to affect the binding activity to any appreciable extent, as small alkyl amides (**24a**), cyclic amides (**24b**, **24c**, **24d**, **24e**), and heteroaromatic amides (**24l**, **24p**, **24q**, **24r**) represented in this group all displayed comparable activity, suggesting orientation into a solvent exposed region of the active site. Introduction of strong electron withdrawing groups on the amide further increased DPP4 binding affinity, as shown in sulfonamides **24i** and **24j** and sulfone **24k**.

Table 1. DPP4/DPP8/DPP9 Inhibition for Compounds **19**, **20**, **21**, and **24a**−**ee**[a]

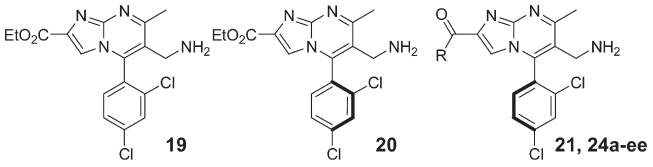

No.	R	DPP4 K_i (nM) DPP8/9 K_i (μM)	No.	R	DPP4 K_i (nM) DPP8/9 K_i (μM)	No.	R	DPP4 K_i (nM) DPP8/9 K_i (μM)
19	(racemic)	0.7 3.9/5.2	**24j**	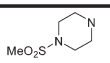	0.5 0.42/0.83	**24u**	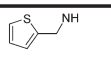	3.2 2.5/5.6
20	(chiral)	11.7 >30/>30	**24k**		0.3 2.2/2.0	**24v**	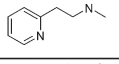	0.7 0.95/0.55
21	OEt (chiral)	0.4 1.9/3.3	**24l**		0.9 0.7/0.9	**24w**	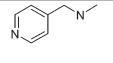	2.6 1.1/0.86
24a		2.4 1.7/1.4	**24m**		6.6 2.3/3.5	**24x**	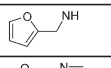	4.0 1.4/3.5
24b		2.9 2.2/1.0	**24n**		2.0 2.9/2.5	**24y**	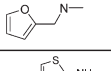	0.9/1.2
24c		2.2 2.4/2.2	**24o**		0.6 1.1/0.94	**24z**	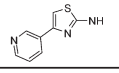	5.0 0.65/1.9
24d		3.1 2.2/1.5	**24p**		1.8 4.1/5.8	**24aa**	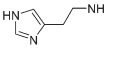	4.7 2.2/3.3
24e	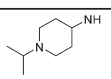	5.0 >10/>10	**24q**		3.8 1.7/2.5	**24bb**	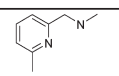	5.4 0.086/0.28
24f	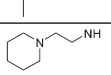	8.7 13/>30	**24r**		2.6 0.4/0.6	**24cc**	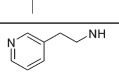	1.5 0.6/0.3
24g		1.0 2.8/1.9	**24s**		1.1 1.3/0.9	**24dd**	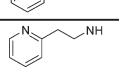	1.4 0.27/0.19
24h		3.1 1.3/1.3	**24t**	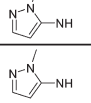	2.0 4.5/3.5	**24ee**	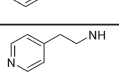	1.3 0.58/2.1
24i	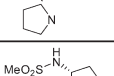	0.2 2.0/2.2						

[a] Values represent the mean of multiple determinations.

In particular, methyl sulfonamide amide **24i** is the most potent compound prepared in this series, with DPP4 K_i of 0.2 nM.

We initially focused on the very potent sulfonamide **24i** for additional biological evaluation. As a TFA salt, **24i** showed excellent aqueous solubility with calculated cLogP of 1.15. While the strong hydrophilicity provided an advantage in terms of formulation for preclinical animal studies, we questioned if this molecule might be too polar to cross biological membranes. When **24i** was tested in caco-2 cell monolayer and parallel membrane permeability assays (PAMPA), very low permeability values of <15 and 0 nm/s, respectively, were obtained, suggestive of no membrane permeability for this compound.[16] Additionally, after a 3 mg/kg oral dose in *ob*/*ob* mice for **24i**, C_{max} at 1 h was 45 nM, likely insufficient for any PD effect despite its high potency. It was further confirmed that when **24i** was administered orally in *ob*/*ob* mice for an oral glucose tolerance test (oGTT), there was no reduction in glucose excursion. Similar lack of in vivo efficacy was observed for other potent and polar compounds, including sulfonamide **24j** and sulfone **24k**. While these analogues were the most potent DPP4 inhibitors from the series, they were also the most polar molecules, with cLogP's in the range of 1−2, which likely contributed to their low permeability. It was reasoned that an increase of lipophilicity by removing some polar functional groups on these molecules may lead to higher permeability across the membranes. Thus, less polar amides were synthesized and evaluated. It was discovered that most of the amides lacking additional polar sulfonamide, amine, or sulfone functionality displayed high PAMPA permeability. For example, comparing **24b** with **24i**, removal of methyl sulfonamide from **24i** decreased DPP4 binding activity by 10-fold but increased PAMPA permeability significantly from unmeasurable to 518 nm/s. Heterocyclic amides such as **24l** and **24s** also showed excellent PAMPA permeabilities of 587 and 669 nm/s, respectively, with morpholino amide **24c** measuring 464 nm/s in the same assay.

Having identified membrane permeability as one prerequisite for efficacy, these compounds were tested for other related peptidase activities. DPP4 belongs to a larger family of peptidases including DPP8,[17] DPP9,[18] DPP2,[19] and fibroblast activation protein (FAP).[20] While all members of the DPP family preferentially cleave Xaa-Pro- and Xaa-Ala- dipeptides (where Xaa is any amino acid except proline) from the N-terminus of proteins, however, the physiological substrates and clinical relevance of these related peptidases have not been definitively established[21] except for DPP4. To date, compounds with varying degrees of selectivity for DPP4 versus DPP8 and DPP9 have been studied in a human clinical setting and are well tolerated. As we continue to explore novel chemical scaffolds directed against this promising target for chronic treatment for type 2 diabetes, selectivity over the other DPPs was nonetheless incorporated into these next generation inhibitors as a medicinal chemistry goal. All of the amides **24a**−**ee** were highly selective for DPP4 over DPP2 and FAP, however, varying degrees of selectivity over DPP8 and DPP9 were observed in this series (Table 1). Esters and alkyl amides were most selective over DPP8 and DPP9, with selectivity ratios typically greater than 1000-fold. For the very potent sulfonamide amide **24i**, the selectivity for DPP4 over DPP8 and DPP9 is approaching 10000-fold. On the other hand, pyridine containing amides **24r**, **24w**, and **24bb**−**24ee** are often less than 500-fold selective for DPP4, suggesting the pyridine ring may have an additional interaction with DPP8 and DPP9 at the corresponding region of the active site. Compound **24bb** is the most potent analogue from this series against DPP8 and DPP9, with selectivity for DPP4 of only 16- and 52-fold, respectively. Selectivity for five-membered ring heteroaromatic amides varied from 500- to 2000-fold, mostly due to their varying degrees of activity at DPP4. By selecting compounds with appropriate DPP4 potency from this subgroup, 1000-fold selectivity can be achieved as shown in amides such as **24s**.

As reported earlier,[14] when the azolo ring of the azolopyrimidine core was substituted with an aromatic or heteroaromatic group (**5**, Figure 1), the analogues displayed significant hERG and sodium channel activities. Various predictive binding models for hERG have been developed, and based on in silico modeling predictions for hERG channel blockers, molecular features that may contribute to increased hERG inhibitory activity include hydrophobicity, high molecular weight, the presence of a basic group such as an amine, and a V-shape topology arising from ring-linker arrangements.[22] Compound **5** contains several of these structural attributes which may explain its high hERG activity. To disrupt some of these features that may contribute to the hERG activity, we explored the SAR off of the five-membered ring of the heterobicyclic core by replacing the pendant aromatic or heteroaromatic system with more polar functionality. It was reasoned that modifications of this type should increase the overall polarity of the analogues and reduce the number of aromatic systems, thereby destroying the resulting V-shaped arrangement. Indeed, when the phenyl ring on **5** was replaced with a more polar ester or amide group, the compounds in general showed reduced ion channel activities. Notably, ester **19** had 23% inhibition for hERG at 10 μM, compared with 74% for **5**. Within the amide series, when a heterocycle such as pyrazole is present in the amide portion of the molecule, the analogues also showed improvement in channel activities compared with the corresponding nonamides. For example, pyrazole amide **24s** had 31% and 2% inhibition for hERG and sodium channel at 10 μM, respectively.

To achieve better understanding of the binding mode, we were able to obtain X-ray crystal structures of both the DPP4 *apo* enzyme and DPP4 bound as a cocrystal with inhibitor **24c** in the active site (Figure 3).[23] Consistent with earlier reports in the literature,[24] the DPP4 binding pocket is located at the interface of the α/β-hydrolase and β-propeller domains. The catalytic triad (S630, H740, and D708), which is highly conserved in the DPP4 gene family (including DPP8 and DPP9), resides in the α/β-hydrolase domain. On the other hand, E205 and E206, which typically interact with the N-terminus of DPP substrates, are located in the β-propeller domain, which is less conserved across the DPP4 gene family. From analysis of the X-ray crystal structure of **24c** bound to DPP4, it is clearly demonstrated that this compound binds in the active site with the 2,4-dichlorophenyl group fitting tightly into the hydrophobic S1 pocket, whereas the primary benzylic amino group forms salt bridges to E205 and E206. The amine also exhibited hydrogen binding interactions with Y662. These key interactions anchor the molecule into the DPP4 binding site and also serve to explain why the alternate orientation of amine and dichlorophenyl groups in the opposite atropisomer would not fit well in this binding mode, leading to weakened binding affinity. Consistent with our observed SAR for this series, the amide portion of the molecule projects to a large, solvent-exposed area of the enzyme pocket, which can tolerate a variety of different groups, including those with polar functionality. Unlike dipeptide mimetic DPP4 inhibitors such

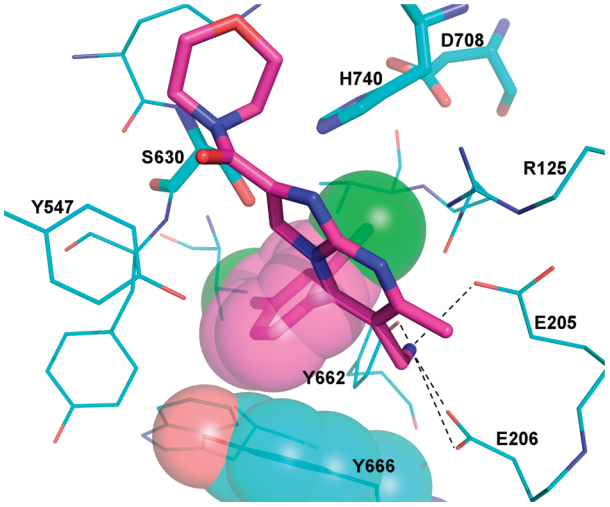

Figure 3. X-ray crystal structure of **24c** and DPP4.

Table 2. PK Profiles for **24c** and **24s**[a]

compd/species	V_{ss} L/kg	$t_{1/2}$ h	CL (iv) mL/min/kg	% of parent in urine	F %
24c/rat	1.3	1.6	25.4	56−79	54
24s/rat	3.9	2.1	43.2	4.4−5.9	64
24c/dog	1.5	4.6	7.9	41	76

[a] Dose: IA: 5 μmol/kg, po: 2 μmol/kg.

as saxagliptin and vildagliptin, where the hydroxy group of S630 from the catalytic triad plays a crucial role in binding, there was no obvious interaction of this catalytic residue with **24c**, and combined with the fact that most of the key contacts with and subsequent binding energy from **24c** within the active site of DPP4 derives from residues in the β-propeller domain, this may help to explain why this chemotype provides high degree of selectivity for DPP4 over DPP8 and DPP9.[25]

On the basis of their highly potent and selective DPP4 inhibitory activity, as well as favorable permeability and low off-target activity, **24c** and **24s** were carried on for additional PK evaluation in preclinical animal models. Key parameters obtained from rat PK studies for **24c** and **24s** after a 5 μmol/kg intraarterial (IA) and 2 μmol/kg oral dose are summarized in Table 2. The vehicle for these studies is water, in which these compounds are freely soluble, another favorable drugability property shared by the present class of compounds. The C_{max} for **24c** at 0.6 h is 324 nM with an $AUC_{0-\infty}$ of 714 nM·h. The systemic plasma clearance of **24c** and **24s** were 25.4 and 43.2 mL/min/kg, respectively, indicating high clearance in rats. The fraction of dose excreted in urine collected from the rats over a 24 h period, as unchanged parent compound was 56−79% for **24c** and 4.4−5.9% for **24s**, indicating renal clearance to be significant for **24c**. The steady state volume of distribution was 1.3 and 3.9 L/kg for **24c** and **24s**. The estimated terminal elimination half-life after IA administration was 1.6 and 2.1 h for **24c** and **24s**, respectively. Despite the relatively high clearance, the absolute oral bioavailability for **24c** and **24s** were excellent at 54 and 64%. Compound **24c** was also evaluated in dog PK profiling with 76% bioavailability and a $t_{1/2}$ of 4.6 h that may be suitable for once-a-day dosing.

An *ob*/*ob* mouse model was utilized to evaluate the in vivo PD effects in an oGTT. In this model, compounds were administered orally in water to the mice 1 h prior to an oral glucose (2 g/kg) bolus. Blood glucose and insulin levels were monitored at different time intervals from 0 to 2 h. At 1 and 3 μmol/kg, **24c** significantly reduced glucose excursion at 15 min by 66% and 63%, respectively. In the same experiment, **24s** reduced glucose excursion up to 40% and 58% after 1 and 3 μmol/kg oral dosing with concurrent increase of insulin AUC 0−2 h by 93% and 129%. In the latter experiment, the plasma DPP4 activity was inhibited by 62% and 52.8%, respectively, after 1 and 3 μmol/kg dosing. The reduced glucose excursion, increase in insulin secretion during an oral glucose challenge, combined with reduced plasma DPP4 activity, supports that DPP4 inhibition was the mechanism for the observed PD effects.

Conclusions

In summary, we have developed a novel series of imidazolopyrimidine amides as potent DPP4 inhibitors. By replacing the aryl substituent on an azolopyrimidine core scaffold from a previously disclosed series with a more polar amide group, the resultant molecules displayed enhanced DPP4 inhibitory activity, as well as markedly reduced hERG and sodium channel activities. Polarity of the compounds was further modified to improve the balance of off-target activity, DPP4 inhibition and plasma exposure levels, leading to amide-containing inhibitors possessing drug-like properties as represented by **24c** and **24s**. X-ray crystallography of **24c** from this class bound to DPP4 confirmed that these compounds bind in the DPP4 binding pocket in a mode consistent with our observed SAR. Lead molecule **24s** from this series demonstrated potent DPP4 activity, selectivity over DPP2, DPP8, and DPP9, low hERG, sodium and calcium ion channel activities, an excellent PK profile in preclinical species, and favorable PD effects. Further evaluation of these compounds as potential treatments for type 2 diabetes is ongoing and will be reported in due course.

Experimental Section

All reactions were carried out under a static atmosphere of argon or nitrogen and stirred magnetically unless otherwise noted. All reagents used were of commercial quality and were obtained from Aldrich Chemical Co., Sigma Chemical Co., Lancaster Chemical Co., or Acros Chemical Co. ^{1}H (400 MHz) and ^{13}C (100 MHz) NMR spectra were recorded on a JEOL GSX400 spectrometer using Me_4Si as an internal standard unless otherwise noted. ^{1}H (500 MHz) and ^{13}C (125 MHz) NMR spectra were recorded on a JEOL JNM-ECP500 spectrometer. Chemical shifts are given in parts per million (ppm) downfield from internal reference Me_4Si in δ units, and coupling constants (J values) are given in hertz (Hz). Selected data are reported in the following manner: chemical shift, multiplicity, coupling constants. All reactions were carried out using commercially available anhydrous solvents from Aldrich Chemical Co. or EM Science Chemical Co. unless otherwise noted. All flash chromatographic separations were performed using E. Merck silica gel (particle size, 0.040−0.063 mm). Reactions were monitored by TLC using 0.25 mm E. Merck silica gel plates (60 F_{254}) and were visualized with UV light, with 5% phosphomolybdic acid in 95% EtOH, or by a sequential treatment with 1 N HCl/MeOH followed by ninhydrin staining. LC/MS data were recorded on a Shimadzu LC-10AT equipped with a SIL-10A injector, a SPD-10AV detector, normally operating at 220 nm, and interfaced with a Micromass ZMD mass spectrometer. LC/MS or HPLC retention times, unless otherwise noted, are reported using a Phenomenex Luna C-18 4.6 mm ×50 mm column eluted with a 4 min gradient from 0 to 100% B, where A = 10% MeOH−90% H_2O−0.1% TFA and B = 90% MeOH−10% H_2O−0.1% TFA. All solvents were removed by rotary evaporation under vacuum using a standard rotovap equipped with a dry ice condenser. All filtrations were performed with a vacuum

unless otherwise noted. Purity of all intermediates and final compounds was determined to be >95% by HPLC (Phenomenex Luna C-18 4.6 mm × 50 mm column eluted with a 4 min gradient from 0 to 100% B, where A = 10% MeOH−90% H_2O−0.1% TFA and B = 90% MeOH−10% H_2O−0.1% TFA and detection at 220 nm) and/or elemental analyses.

***E*/*Z*-*tert*-Butyl 2-(2,4-dichlorobenzylidene)-3-oxobutanoate (8).** To a stirred solution of *tert*-butylacetoacetate **6** (1.50 g, 9.48 mmol) and 2,4-dichlorobenzaldehyde **7** (1.66 g, 9.48 mmol) in 2-propanol (10 mL) was added acetic acid (23.9 μL, 0.400 mmol) and dimethyl amine (2 M solution in THF, 200 μL, 0.400 mmol). The reaction was kept at RT for 3 days and was concentrated under reduced pressure. The resulting yellow oil was purified by silica gel chromatography (0−5% EtOAc in hexanes) to obtain **8** (2.03 g, 67%) as a 1:1 mixture of *E*/*Z* isomers. On the basis of NOE experiments, the *Z* isomer is the slower moving compound on thin layer chromatography (100% hexanes, R_f = 0.60) and the *E* isomer is the faster moving isomer (100% hexanes, R_f = 0.70). For *Z* isomer: ^{1}H NMR (400 MHz, $CDCl_3$) δ 7.68 (s, 1H), 7.49 (d, *J* = 8.4 Hz, 1H), 7.47 (d, *J* = 2.2 Hz, 1H), 7.24 (dd, *J* = 2.2, 7.3 Hz, 1H), 2.44 (s, 3H), 1.45 (s, 9H). ^{13}C NMR (125 MHz, $CDCl_3$) δ 194.5, 165.8, 138.0, 136.4, 135.4, 135.3, 130.8, 130.2, 129.7, 127.0, 83.2, 27.8, 26.9. Anal. Calcd for $C_{15}H_{16}Cl_2O_3$: C, 57.16; H, 5.11; Found: C, 57.26; H, 4.93. For *E* isomer: ^{1}H NMR (400 MHz, $CDCl_3$) δ 7.75 (s, 1H), 7.45 (d, *J* = 2.2 Hz, 1H), 7.28 (d, *J* = 8.3 Hz, 1H), 7.21 (dd, *J* = 2.2, 8.3 Hz, 1H), 2.26 (s, 3H), 1.55 (s, 9H). ^{13}C NMR (125 MHz, $CDCl_3$) δ 202.0, 162.8, 138.4, 136.2, 135.1, 135.0, 130.8, 130.4, 129.7, 127.3, 82.7, 31.1, 27.9. Anal. Calcd for $C_{15}H_{16}Cl_2O_3$: C, 57.16; H, 5.11; Found: C, 57.34; H, 5.04.

Ethyl Imidazo[1,2-*a*]pyrimidine-2-carboxylate (11a) and Ethyl Imidazo[1,2-*a*]pyrimidine-3-carboxylate (11b). 2-Aminopyrimidine **9** (5.00 g, 52.6 mmol) and ethyl bromopyruvate **10** (90%, 7.35 mL, 52.6 mmol) were dissolved in ethanol (80 mL) and heated to 75 °C for 16 h. The reaction was concentrated under reduced pressure and diluted with CH_2Cl_2 and satd aq $NaHCO_3$. The organic layer was washed with satd aq $NaHCO_3$ (2×), and the aq layers were extracted with CH_2Cl_2 (3×). The combined organic layers were dried over $MgSO_4$ and concentrated under reduced pressure. The resulting brown oil was suspended in cold CH_2Cl_2 and filtered. The filter cake was washed with cold CH_2Cl_2 to obtain **11a** (3.02 g, 30%) as a light-yellow solid. The mother liquor contains a mixture of **11a** and **11b** (6.03 g, 60%), which was first purified by silica gel chromatography followed by recrystallization from EtOAc to obtain **11b** (2.04 g, 20%). For 2-isomer **11a**: ^{1}H NMR (500 MHz, $CDCl_3$) δ 8.69 (dd, *J* = 2.2, 6.6 Hz, 1H), 8.67 (dd, *J* = 2.2, 4.4 Hz, 1H), 8.22 (s, 1H), 7.01 (dd, *J* = 3.9, 6.6 Hz, 1H), 4.46 (q, *J* = 7.2 Hz, 2H), 1.43 (t, *J* = 7.2 Hz, 3H). ^{13}C NMR (125 MHz, $CDCl_3$) δ 162.8, 152.2, 147.8, 137.7, 134.4, 115.3, 110.0, 61.2, 14.2. Anal. Calcd for $C_9H_9N_3O_2$: C, 56.54; H, 4.74; N, 21.97; Found: C, 56.25; H, 4.61; N, 21.96. For 3-isomer **11b**: ^{1}H NMR (500 MHz, $CDCl_3$) δ 9.57 (dd, *J* = 2.2, 7.2 Hz, 1H), 8.74 (dd, *J* = 2.2, 4.4 Hz, 1H), 8.45 (s, 1H), 7.17 (dd, *J* = 4.4, 7.2 Hz, 1H), 4.44 (q, *J* = 7.2 Hz, 2H), 1.44 (t, *J* = 7.2 Hz, 3H). ^{13}C NMR (125 MHz, $CDCl_3$) δ 160.1, 152.0, 150.7, 142.4, 135.3, 114.3, 110.3, 60.7, 14.2. Anal. Calcd for $C_9H_9N_3O_2$: H, 4.74; N, 21.97; Found: H, 4.55; N, 22.20.

Ethyl 2-Amino-1*H*-imidazole-4-carboxylate (12). To a stirred solution of **11a** or **11b** (1.00 g, 5.23 mmol) in ethanol (40 mL) was added hydrazine monohydrate (0.284 mL, 5.75 mmol). The reaction was heated to 75 °C for 16 h and was concentrated under reduced pressure. The resulting light-yellow solid was suspended in diethyl ether and filtered to collect **12** (810 mg, 100%) as a white solid. ^{1}H NMR (400 MHz, CD_3OD) δ 7.27 (s, 1H), 4.24 (q, *J* = 7.0 Hz, 2H), 1.31 (t, *J* = 7.0 Hz, 3H). ^{13}C NMR (125 MHz, CD_3OD) δ 165.5, 156.1, 131.8, 125.7, 63.8, 17.3. Anal. Calcd for $C_6H_9N_3O_2$: C, 46.44; H, 5.84; N, 27.08; Found: C, 46.17; H, 5.65; N, 27.28.

6-*tert*-Butyl 2-Ethyl 5-(2,4-dichlorophenyl)-7-methyl-5,8-dihydroimidazo[1,2-*a*]pyrimidine-2,6-dicarboxylate (13). Compounds **12** (980 mg, 6.32 mmol) and **8** (2.03 g, 6.44 mmol) were dissolved in ethanol (15 mL) and heated to 75 °C for 16 h. The reaction was concentrated under reduced pressure to obtain a 10:1 mixture (by HPLC) of **13** and isomeric 6-*tert*-butyl 3-ethyl 5-(2,4-dichlorophenyl)-7-methyl-5,8-dihydroimidazo[1,2-*a*]pyrimidine-3,6-dicarboxylate **3**-isomer (3.07 g) as a yellow foam. A small amount of this mixture (350 mg) was purified by silica gel chromatography to obtain **13** (191 mg, 59%) and **3**-isomer (19.2 mg, 5.9%) as white solids. For 2-isomer **13**: ^{1}H NMR (400 MHz, $CDCl_3$) δ 10.19 (br s, 1H), 7.43 (d, *J* = 2.2 Hz, 1H), 7.38 (s, 1H), 7.34 (d, *J* = 7.2 Hz, 1H), 7.21 (dd, *J* = 2.2, 7.2 Hz, 1H), 6.67 (s, 1H), 4.29 (m, 2H), 2.57 (s, 3H), 1.34 (t, *J* = 7.0 Hz, 3H), 1.26 (s, 9H). ^{13}C NMR (125 MHz, $CDCl_3$) δ 164.6, 162.2, 148.1, 141.6, 138.6, 134.6, 132.9, 130.1, 130.0, 129.2, 128.0, 119.7, 80.2, 60.4, 54.5, 28.1, 19.0, 14.3. Anal. Calcd for $C_{21}H_{23}Cl_2N_3O_4$: C, 55.76; H, 5.12; N, 9.29; Found: C, 55.49; H, 5.04; N, 8.99. HRMS: Anal. Calcd. for $C_{21}H_{24}Cl_2N_3O_4$ 452.1144; Found: 452.1128 $(M + H)^+$.

6-*tert*-Butyl 2-Ethyl 5-(2,4-dichlorophenyl)-7-methylimidazo-[1,2-*a*]pyrimidine-2,6-dicarboxylate (14). To a stirred solution of **13** (191 mg, 0.422 mmol) in acetone (5 mL) was added $KMnO_4$ (66.7 mg, 0.422 mmol). After 1 h, the reaction was filtered through Celite and concentrated under reduced pressure. The resulting residue was diluted with CH_2Cl_2 and extracted with H_2O (2×). The organic layer was dried over $MgSO_4$, concentrated under reduced pressure, and recrystallized from EtOAc to obtain **14** (108 mg, 57%) as white crystals. ^{1}H NMR (400 MHz, $CDCl_3$) δ 7.68 (d, *J* = 1.8 Hz, 1H), 7.53 (s, 1H), 7.50 (dd, *J* = 1.8, 7.6 Hz, 1H), 7.35 (d, *J* = 7.6 Hz, 1H), 4.43 (m, 2H), 2.77 (s, 3H), 1.41 (t, *J* = 7.2 Hz, 3H), 1.29 (s, 9H). ^{13}C NMR (100 MHz, $CDCl_3$) δ 163.7, 162.7, 159.8, 147.0, 141.1, 138.5, 138.2, 134.5, 131.4, 130.3, 128.1, 127.8, 119.0, 114.1, 83.8, 61.4, 27.7, 24.3, 14.3. Anal. Calcd for $C_{21}H_{21}Cl_2N_3O_4$: C, 56.01; H, 4.70; N, 9.33; Found: C, 55.79; H, 4.43; N, 9.14.

5-(2,4-Dichlorophenyl)-2-(ethoxycarbonyl)-7-methylimidazo-[1,2-*a*]pyrimidine-6-carboxylic Acid (15). To a stirred solution of **14** (1.14 g, 2.53 mmol) in CH_2Cl_2 (5 mL) was added TFA (5 mL). The reaction was heated to 60 °C for 30 h and concentrated under reduced pressure to obtain **15** (0.998 g, 100%) as yellow oil. ^{1}H NMR (400 MHz, $CDCl_3$) δ 7.80 (d, *J* = 1.3 Hz, 1H), 7.65 (s, 1H), 7.59 (d, *J* = 1.3 Hz, 2H), 4.36 (q, *J* = 7.0 Hz, 2H), 2.78 (s, 3H), 1.36 (t, *J* = 7.0 Hz, 3H). ^{13}C NMR (100 MHz, $CDCl_3$) δ 161.4, 157.9, 154.9, 142.7, 138.0, 134.6, 133.2, 129.6, 127.8, 125.9, 124.8, 124.0, 113.7, 109.9, 56.0, 25.2, 9.6. Anal. Calcd for $C_{17}H_{13}Cl_2N_3O_4$: C, 51.79; H, 3.32; N, 10.66; Found: C, 51.57; H, 3.05; N, 10.42.

Ethyl 5-(2,4-Dichlorophenyl)-6-(hydroxymethyl)-7-methylimidazo-[1,2-*a*]pyrimidine-2-carboxylate (16). To a stirred solution of **15** (0.998 g, 2.53 mmol) in THF (10 mL) was added ClCOOEt (0.289 mL, 3.04 mmol) and Et_3N (0.529 mL, 3.80 mmol). After 2 h, the reaction was filtered and concentrated under reduced pressure to obtain the mixed anhydride (1.18 g) as brown oil. To a stirred solution of crude mixed anhydride (1.18 g, 2.53 mmol) in THF (10 mL) at 0 °C was added $NaBH_4$ (144 mg, 3.80 mmol) in H_2O (0.5 mL). After 1 h, the reaction was quenched by 1N HCl and diluted with EtOAc. The organic layer was extracted with 1N HCl, satd aq NH_4Cl, and brine before drying over $MgSO_4$. Filtration, concentration under reduced pressure and purification by silica gel chromatography gave **16** (430 mg, 45%) as a light-yellow solid. ^{1}H NMR (400 MHz, $CDCl_3$) δ 7.70 (d, *J* = 7.9 Hz, 1H), 7.63 (d, *J* = 1.8 Hz, 1H), 7.49 (dd, *J* = 1.8, 7.9 Hz, 1H), 7.36 (s, 1H), 4.68 (d, *J* = 12.3 Hz, 1H), 4.36 (m, 3H), 2.75 (s, 3H), 1.35 (t, *J* = 7.0 Hz, 3H). ^{13}C NMR (100 MHz, $CDCl_3$) δ 164.5, 162.6, 147.0, 140.8, 137.8, 136.3, 134.1, 132.7, 130.1, 128.4, 127.1, 121.4, 113.8, 61.1, 57.9, 23.5, 14.2. Anal. Calcd for $C_{17}H_{15}Cl_2N_3O_3$: C, 53.70; H, 3.97; N, 11.05; Found: C, 53.48; H, 3.65; N, 10.80.

Ethyl 6-(Chloromethyl)-5-(2,4-dichlorophenyl)-7-methylimidazo-[1,2-*a*]pyrimidine-2-carboxylate (17). To a stirred solution of **16** (430 mg, 1.13 mmol) in CH_2Cl_2 (10 mL) was added MsCl (0.105 mL, 1.36 mmol) and Et_3N (0.236 mL, 1.70 mmol). After 10 h,

the reaction was concentrated under reduced pressure and diluted with EtOAc. The mixture was extracted with H_2O and brine before drying over $MgSO_4$. Filtration and concentration under reduced pressure gave **17** (448 mg) as yellow oil. ^{1}H NMR (400 MHz, $CDCl_3$) δ 7.72 (d, J = 2.2 Hz, 1H), 7.57 (dd, J = 2.2, 8.4 Hz, 1H), 7.46 (d, J = 8.4 Hz, 1H), 7.45 (s, 1H), 4.53 (d, J = 12.3 Hz, 1H), 4.43 (m, 2H), 4.23 (d, J = 12.3 Hz, 1H), 2.86 (s, 3H), 1.40 (t, J = 7.5 Hz, 3H). ^{13}C NMR (100 MHz, $CDCl_3$) δ 162.8, 162.1, 147.1, 141.4, 138.6, 137.9, 134.2, 131.6, 130.8, 128.7, 126.4, 118.4, 114.0, 61.3, 39.5, 23.3, 14.2. Anal. Calcd for $C_{17}H_{14}Cl_3N_3O_2$: C, 51.21; H, 3.53; N, 10.54; Found: C, 50.92; H, 3.45; N, 10.25.

Ethyl 6-(Azidomethyl)-5-(2,4-dichlorophenyl)-7-methylimidazo-[1,2-*a*]pyrimidine-2-carboxylate (18). To a stirred solution of crude **17** (448 mg, 1.12 mmol) in DMF (5 mL) was added NaN_3 (110 mg, 1.69 mmol). The reaction was heated to 50 °C for 1 h. After cooling, the reaction was diluted with EtOAc and extracted with H_2O and brine before drying over $MgSO_4$. Filtration and concentration under reduced pressure gave **18** (450 mg) as yellow oil. ^{1}H NMR (400 MHz, $CDCl_3$) δ 7.72 (d, J = 2.2 Hz, 1H), 7.59 (dd, J = 2.2, 7.2 Hz, 1H), 7.43 (s, 1H), 7.43 (d, J = 7.0 Hz, 1H), 4.41 (m, 2H), 4.31 (d, J = 14.0 Hz, 1H), 4.18 (d, J = 14.0 Hz, 1H), 2.79 (s, 3H), 1.40 (t, J = 7.0 Hz, 3H). ^{13}C NMR (125 MHz, $CDCl_3$) δ 162.7, 162.3, 147.1, 141.5, 138.6, 137.7, 134.3, 132.0, 130.7, 128.7, 126.5, 116.5, 113.9, 61.2, 48.1, 23.6, 14.2. Anal. Calcd for $C_{17}H_{14}Cl_2N_6O_2$: C, 50.38; H, 3.48; N, 20.73; Found: C, 50.33; H, 3.47; N, 20.66.

Ethyl 6-(Aminomethyl)-5-(2,4-dichlorophenyl)-7-methylimidazo-[1,2-*a*]pyrimidine-2-carboxylate (19). To a stirred solution of **18** (450 mg, 1.11 mmol) in THF (10 mL) and H_2O (0.5 mL) was added PPh_3 polymer bound (3 mmol/g, 750 mg, 2.25 mmol). The reaction was heated to 50 °C for 24 h. The reaction was filtered and concentrated to give crude **19** (315 mg, 74% crude yield) as yellow oil. A part (115 mg) was purified by reverse phase preparatory HPLC to give **19**, TFA salt (102 mg, 50% for 3 steps) as a white solid. ^{1}H NMR (400 MHz, CD_3OD) δ 7.94 (d, J = 1.8 Hz, 1H), 7.75 (dd, J = 1.8, 8.3 Hz, 1H), 7.64 (s, 1H), 7.63 (d, J = 8.3 Hz, 1H), 4.36 (q, J = 7.0 Hz, 2H), 4.18 (d, J = 14.9 Hz, 1H), 4.02 (d, J = 14.9 Hz, 1H), 2.83 (s, 3H), 1.35 (t, J = 7.0 Hz, 3H). HRMS: Anal. Calcd for $C_{17}H_{17}Cl_2N_4O_2$ 379.0729; Found: 379.0736 $(M + H)^+$.

(−)- and (+)-Ethyl 6-(aminomethyl)-5-(2,4-dichlorophenyl)-7-methylimidazo[1,2-*a*]pyrimidine-2-carboxylate (20) and (21). For **20** and **21**, 50 mg of **19** was separated on a chiral OJ column (15% B isocratic, 20 min, A = heptane, B = MeOH-EtOH (1:1) with 0.1% DEA) to obtain **20** (15 mg, 86.5% ee) $[\alpha]^{24.6}_D$ −25.8° (*c* 3.15, MeOH) and **21** (17 mg, 88.5% ee) $[\alpha]^{24.9}_D$ +24.9° (*c* 3.11, MeOH). For (−) isomer **20**, ^{1}H NMR (400 MHz, CD_3OD) δ 7.93 (d, J = 2.2 Hz, 1H), 7.74 (dd, J = 2.2, 8.3 Hz, 1H), 7.64 (d, J = 8.3 Hz, 1H), 7.62 (s, 1H), 4.36 (q, J = 7.0 Hz, 2H), 4.18 (d, J = 14.9 Hz, 1H), 4.02 (d, J = 14.9 Hz, 1H), 2.82 (s, 3H), 1.35 (t, J = 7.0 Hz, 3H). ^{13}C NMR (100 MHz, CD_3OD) δ 164.1, 163.3, 162 (TFA), 147.9, 144.2, 139.3, 137.8, 134.7, 133.0, 131.5, 129.9, 127.0, 120 (TFA), 116.7, 115.3, 61.8, 36.8, 23.6, 14.1. For (+) isomer **21**, ^{1}H NMR (400 MHz, CD_3OD) δ 7.94 (d, J = 2.2 Hz, 1H), 7.74 (dd, J = 2.2, 8.4 Hz, 1H), 7.63 (d, J = 8.4 Hz, 1H), 7.62 (s, 1H), 4.36 (q, J = 7.5 Hz, 2H), 4.17 (d, J = 14.5 Hz, 1H), 4.02 (d, J = 14.5 Hz, 1H), 2.82 (s, 3H), 1.35 (t, J = 7.5 Hz, 3H). ^{13}C NMR (100 MHz, CD_3OD) δ 163.3, 162.3, 147.5, 143.6, 138.7, 137.5, 134.0, 132.2, 130.9, 129.2, 126.2, 115.7, 114.6, 61.1, 36.2, 22.8, 13.3.

(+)-Ethyl 6-(Azidomethyl)-5-(2,4-dichlorophenyl)-7-methylimidazo[1,2-*a*]pyrimidine-2-carboxylate (22). 10.0 g of racemate **18** was separated by supercritical fluid chromatography on Chiralpak OF, 250 mm × 20 mm, 10 μm, at 35 °C, 50 mL/min; mobile phase, CO_2/MeOH/DEA, 65/35/0.1; injection volume, 3.5 mL of 33 mg/mL sample solution; detector wavelength, 220 nm to obtain (−)-ethyl 6-(azidomethyl)-5-(2,4-dichlorophenyl)-7-methylimidazo[1,2-*a*]pyrimidine-2-carboxylate (5.00 g, 50%) and **22** (5.00 g, 50%) as white solids. For (+)-isomer **22**: HPLC Chiralpak OF, 4.6 mm × 250 mm, 10 μm; isocratic CO_2/MeOH/DEA, 60/40/0.1 over 25 min, 2.0 mL/min; t_R = 17.94 min; 100% homogeneity index, >99.9% ee. ^{1}H NMR (400 MHz, $CDCl_3$) δ 7.72 (d, J = 2.2 Hz, 1H), 7.60 (dd, J = 2.2, 8.3 Hz, 1H), 7.45 (d, J = 8.3 Hz, 1H), 7.43 (s, 1H), 4.40 (q, J = 7.2 Hz, 2H), 4.32 (d, J = 13.8 Hz, 1H), 4.19 (d, J = 13.8 Hz, 1H), 2.78 (s, 3H), 1.39 (t, J = 7.2 Hz, 3H). ^{13}C NMR (100 MHz, $CDCl_3$) δ 162.7, 162.3, 147.1, 141.5, 138.6, 137.8, 134.3, 132.0, 130.8, 128.7, 126.5, 116.5, 113.9, 61.2, 48.1, 23.6, 14.2. Anal. Calcd for $C_{17}H_{14}Cl_2N_6O_2$: C, 50.38; H, 3.48; N, 20.73; Cl, 17.49; Found: C, 50.49; H, 3.58; N, 20.47; Cl, 17.71. HRMS: Anal. Calcd for $C_{17}H_{15}Cl_2N_6O_2$ 405.0628; Found: 405.0640 $(M + H)^+$.

(+)-6-(Azidomethyl)-5-(2,4-dichlorophenyl)-7-methylimidazo-[1,2-*a*]pyrimidine-2-carboxylic Acid (23). To a stirred solution of **22** (1.00 g, 2.47 mmol) in THF (20 mL) and H_2O (2 mL) was added $LiOH \cdot H_2O$ (155 mg, 3.70 mmol). After heating to 50 °C for 16 h, the reaction was concentrated under reduced pressure and diluted with EtOAc. The aqueous layer was acidified by 1N HCl to pH = 1. The organic layer was washed with satd aq NH_4Cl and brine before drying over $MgSO_4$. Filtration and concentration under reduced pressure provided **23** (874 mg, 94%, >99% ee) as a white solid; $[\alpha]^{25}_D$ +77.8° (*c* 2.38, MeOH). ^{1}H NMR (400 MHz, $CDCl_3$) δ 8.71 (br s, 1H), 7.67 (s, 1H), 7.59 (d, J = 8.2 Hz, 1H), 7.55 (d, J = 8.2 Hz, 1H), 7.51 (s, 1H), 4.33 (d, J = 13.8 Hz, 1H), 4.24 (d, J = 13.8 Hz, 1H), 2.79 (s, 3H). ^{13}C NMR (100 MHz, $CDCl_3$) δ 164.1, 163.6, 146.5, 142.0, 138.8, 136.9, 134.2, 132.3, 130.7, 128.9, 126.2, 117.3, 114.4, 48.1, 23.6. Anal. Calcd for $C_{15}H_{10}Cl_2N_6O_2 \cdot 0.1EtOAc \cdot 0.7H_2O$: C, 46.40; H, 3.09; N, 21.08; Found: C, 46.21; H, 2.99; N, 20.93. HRMS: Anal. Calcd for $C_{15}H_{11}Cl_2N_6O_2$ 377.0321; Found: 377.0313 $(M + H)^+$.

(+)-(6-(Azidomethyl)-5-(2,4-dichlorophenyl)-7-methylimidazo-[1,2-*a*]pyrimidin-2-yl)(morpholino)methanone. To a stirred solution of **23** (150 mg, 0.400 mmol) in THF (10 mL) was added morpholine (52.2 μL, 0.597 mmol), HOAt (81.3 mg, 0.597 mmol), EDAC (114 mg, 0.597 mmol), and ^{i}Pr$_2$NEt (138 μL, 0.795 mmol). The reaction was kept at RT for 2 h and was concentrated under reduced pressure. The residue was diluted with EtOAc, and the organic layer was washed with 1N HCl, 1N NaOH, and brine prior to drying over anhydrous $MgSO_4$. Filtration and concentration under reduced pressure afforded the amide (177 mg, 99% crude yield) as a clear glass. A small amount was purified by silica gel chromatography (100% EtOAc) to afford the product (99% purity, >99% ee); $[\alpha]^{25}_D$ +82.7° (*c* 2.26, MeOH). ^{1}H NMR (400 MHz, $CDCl_3$) δ 7.70 (d, J = 2.2 Hz, 1H), 7.56 (dd, J = 2.2, 8.2 Hz, 1H), 7.50 (s, 1H), 7.35 (d, J = 8.2 Hz, 1H), 4.56 (m, 2H), 4.31 (d, J = 14.3 Hz, 1H), 4.18 (d, J = 14.3 Hz, 1H), 3.78 (s, 6H), 2.81 (s, 3H). ^{13}C NMR (100 MHz, $CDCl_3$) δ 161.7, 161.7, 146.0, 141.9, 141.6, 138.7, 134.4, 131.9, 130.8, 128.7, 126.6, 116.2, 114.6, 67.4, 66.9, 48.1, 47.3, 43.2, 23.5. Anal. Calcd for $C_{19}H_{17}Cl_2N_7O_2$: C, 51.13; H, 3.83; N, 21.96; Found: C, 50.97; H, 3.57; N, 21.75.

(+)-(6-(Aminomethyl)-5-(2,4-dichlorophenyl)-7-methylimidazo-[1,2-*a*]pyrimidin-2-yl)(morpholino)methanone (24c). To a stirred solution of the above amide (177 mg, 0.397 mmol) in THF (8 mL) and H_2O (0.8 mL) was added PPh_3 polymer bound (3 mmol/g, 199 mg, 0.600 mmol) and heated to 50 °C for 24 h. The reaction was filtered, concentrated under reduced pressure, and purified by reverse phase HPLC to give **24c**, TFA salt (121 mg, 56% yield, >99% ee) as a white solid; $[\alpha]^{24.3}_D$ +54.12° (*c* 2.62, MeOH). ^{1}H NMR (400 MHz, CD_3OD) δ 7.92 (d, J = 2.2 Hz, 1H), 7.73 (dd, J = 2.2, 8.4 Hz, 1H), 7.62 (d, J = 8.4 Hz, 1H), 7.55 (s, 1H), 4.19 (d, J = 15.0 Hz, 1H), 4.01 (d, J = 15.0 Hz, 1H), 4.01 (br s, 2H), 3.73 (br s, 6H), 2.86 (s, 3H). ^{13}C NMR (100 MHz, CD_3OD) δ 164.6, 164.5, 162 (TFA), 148.1, 145.3, 141.8, 140.5, 135.7, 133.8, 132.6, 130.8, 128.0, 120 (TFA), 117.1, 114.9, 68.2, 44.7, 37.8, 24.2. Anal. Calcd for $C_{19}H_{19}Cl_2N_7O_2 \cdot 1.5TFA$: C, 44.24; H, 3.45; N, 11.62; Found: C, 44.40; H, 3.72; N, 11.90.

In Vitro DPP4 Inhibition Assays. Inhibition of human DPP4 activity was measured under steady-state conditions by following the absorbance increase at 405 nm upon the cleavage of the pseudosubstrate, Gly-Pro-*p*NA. Assays were performed in 96-well plates using a Thermomax plate reader. Typical reactions contained 100 μL of ATE buffer (100 mM Aces, 52 mM

Tris, 52 mM ethanolamine, pH 7.4), 0.45 nM enzyme, either 120 or 1000 μM of substrate ($S < K_m$ and $S > K_m$, $K_m = 180$ μM) and 10 or 11 concentrations of the inhibitor. To ensure steady-state conditions for slow-binding inhibitors, enzyme was pre-incubated with the compound for 40 min prior to substrate addition. All serial inhibitor dilutions were in DMSO and final solvent concentration did not exceed 1%. Inhibitor potency was evaluated by calculating IC_{50}'s at each substrate concentration and then converting them to K_i's by assuming competitive inhibition according to the equation $K_i = IC_{50}/[1 + (S/K_m)]$. All inhibitors were competitive as judged by close agreement of K_i values obtained from assays at high and low substrate concentrations. In cases where IC_{50} at the low substrate concentration was close to the enzyme concentration used in the assay, the data were fit to the Morrison equation to account for the depletion of the free inhibitor.

oGTT in *ob*/*ob* Mice. Male 13−14 week-old *ob*/*ob* mice (Jackson Laboratories) were maintained under constant temperature and humidity conditions, a 12 h/12 h light−dark cycle, and had free access to a 10% fat rodent diet (D1245B Research Diets) and tap water. After an overnight fasting period, animals were dosed orally with vehicle (water) or DPP4 inhibitor (1, 3 μmol/kg) at −60 min. Two blood samples were collected at −60 and 0 min by tail bleed for glucose and insulin determinations. Glucose (2 g/kg) was then administered orally (at 0 min). Additional blood samples were collected at 15, 30, 60, 90, and 120 min for glucose and insulin determinations. Blood samples were collected into EDTA containing tubes (Sarstedt). Plasma glucose was determined with an Accu-Chek Advantage (Roche) glucometer. Plasma insulin was assayed using a mouse insulin ELISA kit (ALPCO Diagnostics). Data represent the mean of 12−24 mice/group. Data analysis was performed using one way ANOVA followed by Dunnett's test. All procedures were performed according to BMS-IACUC guidelines.

Acknowledgment. We thank the Department of Discovery Analytical Sciences at BMS for their assistance in the characterization of the compounds reported herein and for maintenance of various analytical instruments and the Department of Pharmaceutical Candidate Optimization for performing in vitro and in vivo assays to aid in the profiling of these compounds.

Supporting Information Available: ^{1}H and ^{13}C NMR data, and elemental analyses for compounds **24a**, **24b**, **24d**−**24i**, and **24l**−**24ee**. This material is available free of charge via the Internet at http://pubs.acs.org.

References

(1) (a) Wideman, R. D.; Kieffer, T. J. Mining incretin hormone pathways for novel therapies. *Trends Endocrinol. Metab*. **2009**, *20*, 280–286. (b) Triplitt, C.; Wright, A.; Chiquette, E. Incretin mimetics and dipeptidyl peptidase-IV inhibitors: potential new therapies for type 2 diabetes mellitus. *Pharmacotherapy* **2006**, *26*, 360–374. (c) Gallwitz, B. Glucagon-like peptide-1-based therapies for the treatment of type 2 diabetes mellitus. *Treat. Endocrinol*. **2005**, *4*, 361–370.

(2) (a) Holst, J. J. Glucagon-like peptide-1 (GLP-1) a newly discovered GI hormone. *Gastroenterology* **1994**, *107*, 1048–1055. (b) Drucker, D. J. Glucagon-like peptides. *Diabetes* **1998**, *47*, 159–169.

(3) (a) Vilsboll, T.; Holst, J. J. Incretins, insulin secretion and type 2 diabetes mellitus. *Diabetologia* **2004**, *47*, 357–366. (b) Elahi, D.; McAloon-Dyke, M.; Fukagawa, N. K.; Meneilly, G. S.; Sclater, A. L.; Minaker, K. L.; Habener, J. F.; Andersen, D. K. The insulinotropic actions of glucose-dependent insulinotropic polypeptide (GIP) and glucagon-like peptide-1 (7−37) in normal and diabetic subjects. *Regul. Pept*. **1994**, *51*, 63–75. (c) Nauck, M. A.; Bartels, E.; Oerskov, C.; Ebert, R.; Creutzfeldt, W. Additive insulinotropic effects of exogenous synthetic human gastric inhibitory polypeptide and glucagon-like peptide-1-(7−36) amide infused at near-physiological insulinotropic hormone and glucose concentrations. *J. Clin. Endocrinol. Metab*. **1993**, *76*, 912–917.

(4) (a) Gentilella, R.; Bianchi, C.; Rossi, A.; Rotella, C. M. Exenatide: a review from pharmacology to clinical practice. *Diabetes, Obes. Metab*. **2009**, *11*, 544–556. (b) Gonzalez, C.; Beruto, V.; Keller, G.; Santoro, S.; Di Girolamo, G. Investigational treatments for type 2 diabetes mellitus: Exenatide and Liraglutide. *Expert Opin. Invest. Drugs* **2006**, *15*, 887–895.

(5) Holst, J. J. Therapy of type 2 diabetes mellitus based on the actions of glucagon-like peptide-1. *Diabetes Metab. Res. Rev*. **2002**, *18*, 430–441.

(6) Hansen, L.; Deacon, C. F.; Orskov, C.; Holst, J. J. Glucagon-like peptide-1-(7−36)amide is transformed to glucagon-like peptide-1-(9−36)amide by dipeptidyl peptidase IV in the capillaries supplying the L cells of the porcine intestine. *Endocrinology* **1999**, *140*, 5356–5363.

(7) (a) Nagakura, T.; Yasuda, N.; Yamazaki, K.; Ikuta, H.; Yoshikawa, S.; Asano, O.; Tanaka, I. Improved glucose tolerance via enhanced glucose-dependent insulin secretion in dipeptidyl peptidase IV-deficient Fischer rats. *Biochem. Biophys. Res. Commun*. **2001**, *284*, 501–506. (b) Marguet, D.; Baggio, L.; Kobayashi, T.; Bernard, A.; Pierres, M.; Nielsen, P. F.; Ribel, U.; Watanabe, T.; Drucker, D. J.; Wagtmann, N. Enhanced insulin secretion and improved glucose tolerance in mice lacking CD26. *Proc. Natl. Acad. Sci. U.S.A*. **2000**, *97*, 6874–6879.

(8) (a) Durinx, C.; Lambeir, A.; Bosmans, E.; Falmagne, J.; Berghmans, R.; Haemers, A.; Scharpe, S.; De Meester, I. Molecular characterization of dipeptidyl peptidase activity in serum. Soluble CD26/dipeptidyl peptidase IV is responsible for the release of X-Pro dipeptides. *Eur. J. Biochem*. **2000**, *267*, 5608–5613. (b) Iwaki-Egawa, S.; Watanabe, Y.; Kikuya, Y.; Fujimoto, Y. Dipeptidyl peptidase IV from human serum: purification, characterization, and N-terminal amino acid sequence. *J. Biochem*. **1998**, *124*, 428–433.

(9) Villhauer, E. B.; Brinkman, J. A.; Naderi, G. B.; Burkey, B. F.; Dunning, B. E.; Prasad, K.; Mangold, B. L.; Russell, M. E.; Hughes, T. E. 1-[[(3-Hydroxy-1-adamantyl)amino]acetyl]-2-cyano-(*S*)-pyrrolidine: A potent, selective, and orally bioavailable dipeptidyl peptidase IV inhibitor with antihyperglycemic properties. *J. Med. Chem*. **2003**, *46*, 2774–2789.

(10) Kim, D.; Wang, L.; Beconi, M.; Eiermann, G. J.; Fisher, M. H.; He, H.; Hickey, G. J.; Kowalchick, J. E.; Leiting, B.; Lyons, K.; Marsilio, F.; McCann, M. E.; Patel, R. A.; Petrov, A.; Scapin, G.; Patel, S. B.; Roy, R. S.; Wu, J. K.; Wyvratt, M. J.; Zhang, B. B.; Zhu, L.; Thornberry, N. A.; Weber, A. E. (2*R*)-4-Oxo-4-[3-(trifluoromethyl)-5,6-dihydro[1,2,4]triazolo[4,3-*a*]pyrazin-7(8*H*)-yl]-1-(2,4,5-trifluorophenyl)butan-2-amine: a potent, orally active dipeptidyl peptidase IV inhibitor for the treatment of type 2 diabetes. *J. Med. Chem*. **2005**, *48*, 141–151.

(11) Augeri, D. J.; Robl, J. A.; Betebenner, D. A.; Magnin, D. R.; Khanna, A.; Robertson, J. G.; Wang, A.; Simpkins, L. M.; Taunk, P.; Huang, Q.; Han, S. P.; Abboa-Offei, B.; Cap, M.; Xin, L.; Tao, L.; Tozzo, E.; Welzel, G. E.; Egan, D. M.; Marcinkeviciene, J.; Chang, S. Y.; Biller, S. A.; Kirby, M. S.; Parker, R. A.; Hamann, L. G. Discovery and preclinical profile of saxagliptin (BMS-477118): a highly potent, long-acting, orally active dipeptidyl peptidase IV inhibitor for the treatment of Type 2 diabetes. *J. Med. Chem*. **2005**, *48*, 5025–5037.

(12) Feng, J.; Zhang, Z.; Wallace, M. B.; Stafford, J. A.; Kaldor, S. W.; Kassel, D. B.; Navre, M.; Shi, L.; Skene, R. J.; Asakawa, T.; Takeuchi, K.; Xu, R.; Webb, D. R.; Gwaltney, S. L. Discovery of alogliptin: a potent, selective, bioavailable, and efficacious inhibitor of dipeptidyl peptidase IV. *J. Med. Chem*. **2007**, *50*, 2297–2300.

(13) For other small molecular DPP4 inhibitors, see Havale, S. H.; Pal, M. Medicinal chemistry approaches to the inhibition of dipeptidyl peptidase-4 for the treatment of type 2 diabetes. *Bioorg. Med. Chem*. **2009**, *17*, 1783–1802 and references cited therein.

(14) Brigance, R. P.; Meng, W.; Fura, A.; Harrity, T.; Wang, A.; Zahler, R.; Kirby, M. S.; Hamman, L. G. Synthesis and SAR of azolopyrimidines as potent and selective dipeptidyl peptidase-4 (DPP4) inhibitors for type 2 diabetes. *Bioorg. Med. Chem. Lett*. **2010**, *20*, 4395−4398.

(15) (a) Abignente, E.; Sacchi, A.; Laneri, S.; Rossi, F.; D'Amico, M.; Berrino, L.; Calderaro, V.; Parrillo, C. Research on heterocyclic compounds. XXXII. Synthesis and cyclooxygenase-independent antiinflammatory and analgesic activity of imidazo[1,2-*a*]pyrimidine derivatives. *Eur. J. Med. Chem*. **1994**, *29*, 279–286. (b) Commercon, A. Preparation of bis(N-protected)-2-aminoimidazole-4-carboxaldehyde. *Fr. Demande* **1993**, 12 pp. FR 2681323.

(16) Box, K.; Comer, J.; Huque, F. Correlations between PAMPA permeability and log *P*. In *Pharmacokinetic Profiling in Drug Research: Biological, Physicochemical, And Computational Strategies*; Testa, B., Ed.; Verlag Helvetica Chimica Acta: Zurich, Switzerland, 2006; pp 243−257.

(17) (a) Abbott, C. A.; Yu, D. M. T.; Woollatt, E.; Sutherland, G. R.; McCaughan, G. W.; Gorrell, M. D. Cloning, expression and

chromosomal localization of a novel human dipeptidyl peptidase (DPP) IV homolog, DPP8. *Eur. J. Biochem.* **2000**, *267*, 6140–6150. (b) Bjelke, J., R.; Christensen, J.; Nielsen, P., F.; Branner, S.; Kanstrup, A. B.; Wagtmann, N.; Rasmussen, H. B. Dipeptidyl peptidases 8 and 9: specificity and molecular characterization compared with dipeptidyl peptidase IV. *Biochem. J.* **2006**, *396*, 391–399.

(18) (a) Olsen, C.; Wagtmann, N. Identification and characterization of human DPP9, a novel homologue of dipeptidyl peptidase IV. *Gene* **2002**, *299*, 185–193. (b) Ajami, K.; Abbott, C., A.; McCaughan, G., W.; Gorrell, M., D. Dipeptidyl peptidase 9 has two forms, a broad tissue distribution, cytoplasmic localization and DPIV-like peptidase activity. *Biochim. Biophys. Acta* **2004**, *1679*, 18–28.

(19) (a) Maes, M. B.; Lambeir, A. M.; Gilany, K.; Senten, K.; Van der veken, P.; Leiting, B.; Augustyns, K.; Scharpe, S.; De Meester, I. Kinetic investigation of human dipeptidyl peptidase II (DPPII)-mediated hydrolysis of dipeptide derivatives and its identification as quiescent cell proline dipeptidase (QPP)/dipeptidyl peptidase 7 (DPP7). *Biochem. J.* **2005**, *386*, 315–324. (b) Araki, H.; Li, Y. H.; Yamamoto, Y.; Haneda, M.; Nishi, K.; Kikkawa, R.; Ohkubo, I. Purification, molecular cloning, and immunohistochemical localization of dipeptidyl peptidase II from the rat kidney and its identity with quiescent cell proline dipeptidase. *J. Biochem.* **2001**, *129*, 279–288.

(20) (a) Gorrell, M. D.; Yu, D. M. T. Diverse functions in a conserved structure: the dipeptidyl peptidase IV gene family. In *Trends in Protein Research*; Robinson, J. W., Ed.; Nova Science Publishers, Inc.: Hauppauge, NY, 2005; pp 1−78. (b) Edosada, C. Y.; Quan, C.; Wiesmann, C.; Tran, T.; Sutherlin, D.; Reynolds, M.; Elliott, J. M.; Raab, H.; Fairbrother, W.; Wolf, B. B. Selective inhibition of fibroblast activation protein protease based on dipeptide substrate specificity. *J. Biol. Chem.* **2006**, *281*, 7437–7444.

(21) (a) Burkey, B. F.; Hoffmann, P. K.; Hassiepen, U.; Trappe, J.; Juedes, M.; Foley, J. E. Adverse effects of dipeptidyl peptidases 8 and 9 inhibition in rodents revisited. *Diabetes Obes. Metab.* **2008**, *10*, 1057–1061. (b) Lankas, G. R.; Leiting, B.; Roy, R. S.; Eiermann, G. J.; Beconi, M. G.; Biftu, T.; Chan, C. C.; Edmondson, S.; Feeney, W. P.; He, H.; Ippolito, D. E.; Kim, D.; Lyons, K. A.; Ok, H. O.; Patel, R. A.; Petrov, A. N.; Pryor, K. A.; Qian, X.; Reigle, L.; Woods, A.; Wu, J. K.; Zaller, D.; Zhang, X.; Zhu, L.; Weber, A. E.; Thornberry, N. A. Dipeptidyl peptidase IV inhibition for the treatment of type 2 diabetes. Potential importance of selectivity over dipeptidyl peptidases 8 and 9. *Diabetes* **2005**, *54*, 2988–2994.

(22) (a) Aronov, A. M. Predictive in silico modeling for hERG channel blockers. *Drug Discovery Today* **2005**, *10*, 149–155. (b) Song, M.; Clark, M. Development and evaluation of an in silico model for hERG binding. *J. Chem. Inf. Model* **2006**, *46*, 392–400. (c) Vaz, R. J.; Li, Y.; Rampe, D. Human ether-a-go-go related gene (HERG): a chemist's perspective. *Prog. Med. Chem.* **2005**, *43*, 1–18.

(23) The X-ray crystal structure coordinates of **24c** (BMS-762382) in DPP4 are deposited in the Protein Data Bank (PDB code 3NOX).

(24) (a) Metzler, W. J.; Yanchunas, J.; Weigelt, C.; Kish, K.; Klei, H. E.; Xie, D.; Zhang, Y.; Corbett, M.; Tamura, J. K.; He, B.; Hamann, L. G.; Kirby, M. S.; Marcinkeviciene, J. Involvement of DPP-IV catalytic residues in enzyme−saxagliptin complex formation. *Protein Sci.* **2008**, *17*, 240–250. (b) Thoma, R.; Loffler, B.; Stihle, M.; Huber, W.; Ruf, A.; Hennig, M. Structural basis of proline-specific exopeptidase activity as observed in human dipeptidyl peptidase-IV. *Structure* **2003**, *11*, 947–959. (c) Engel, M.; Hoffmann, T.; Wagner, L.; Wermann, M.; Heiser, U.; Kiefersauer, R.; Huber, R.; Bode, W.; Demuth, H.-U.; Brandstetter, H. The crystal structure of dipeptidyl peptidase IV (CD26) reveals its functional regulation and enzymatic mechanism. *Proc. Natl. Acad. Sci. U.S.A.* **2003**, *100*, 5063–5068.

(25) Kirby, M.; Yu, D. M. T.; O'Connor, S. P.; Gorrell, M. D. Inhibitor selectivity in the clinical application of dipeptidyl peptidase-4 inhibition. *Clin. Sci.* **2010**, *118*, 31–41.